Three-dimensional effects influencing failure in bend-free, variable stiffness composite pressure vessels

Three-dimensional Effects Influencing Failure in Bend-free, Variable Stiffness Composite Pressure Vessels

Shahrzad Daghighi[a], Paul M. Weaver[a]

[a]*Bernal Institute, School of Engineering, University of Limerick, Limerick, Ireland*

Abstract

Pressure vessels enable liquids and gases to be stored and transported safely, finding pervasive use in many industries. These types of structure can be manufactured into many different shapes and from various materials to satisfy the requirements of their specific applications. Maximum allowable pressure is an important factor that should be considered carefully in the design process. Bend-free pressure vessels, that are enabled by variable stiffness composite designs, can even out in-plane stress distributions in the through-thickness direction thereby increasing overall load carrying capacity often accompanied by significant weight reduction. Bend-free composite vessels can therefore be considered to be possible candidates for the next generation of pressure vessels and therefore it is important to study their failure performance, often driven by safety reasons.

In this study, the maximum allowable internal pressure is determined for bend-free ellipsoidal pressure vessels exploiting variable stiffness properties, using first-ply failure based on both Tsai-Wu and the recently proposed three-dimensional invariant-based failure criteria with performance subsequently compared against conventional constant stiffness, composite vessels. Parametric studies are then performed to provide physical insight and also to evaluate the effect of various material properties on the difference in failure load prediction found by these criteria.

Nomenclature

β	parameter defining the nonlinearity of the shear stress-shear strain relation
Δ	$\frac{r_\theta}{r_\varphi}$
ν	Poisson's ratio
σ_1, σ_2, τ_{12}	in-plane stresses
θ	curvilinear coordinate in latitudinal direction
θ_1	fibre direction in composite
φ	curvilinear coordinate in longitudinal direction
a	semi-major axis of in super ellipsoid of revolution
b	semi-minor axis of in super ellipsoid of revolution
E	Young's modulus
G	shear modulus
H_1, H_{11}, H_2, H_{22}, H_6, H_{66}, H_{12}	coefficients of Tsai-Wu failure criteria
K	aspect ratio of super ellipsoid of revolution, $\frac{b}{a}$
N	shape parameter in super ellipsoid of revolution
P_{3D}	max allowable internal pressure found by three-dimensional invariant-based failure criterion
P_{TW}	max allowable internal pressure found by Tsai-Wu criterion
$R_{\%}$	failure load reduction percentage
r_θ, r_φ	radii of curvature in φ and θ direction
S_L	in-plane shear strength

U_1, U_2, U_3, U_4	material invariants	Y_T, Y_C	transverse tensile and compressive strengths
V_1^A, V_2^A	in-plane lamination parameters		
X_T, X_C	longitudinal tensile and compressive strengths	Y_{BT}, Y_{BC}	transverse tensile and compressive biaxial strengths

1. Introduction

Pressure vessels are widely used in many industries for storing liquids and gases and for transportation in often harsh environments. They can have a variety of applications from the altitudes of space in rocket structures, to the depths of oceans as submarines. The design of pressure vessels was first referred to by Leonardo da Vinci in 1495 in $Codex Madrid$ where he described how to use containers of pressurised air to lift heavy weights. However, it was during the $1800s$ and $1900s$ that pressurised vessels became widely used when steam became the main source of power [1].

Pressure vessels traditionally are fully made of metal (Type I). Due to their relatively heavy weight and low strength, metal pressure vessels are not suitable for all applications especially, in the transportation industry where fuel consumption and environmental issues are important. Type II describe metallic vessels reinforced with composite layers in the hoop direction, while Type III refer to metallic vessels fully overwrapped with composite layers. Type IV describe plastic liners fully overwrapped with composite layers which notably reduces weight and increases vessel strength. Fully composite vessels, known as Type V, are the most advanced types of pressure vessel used in aerospace applications [2].

Type V pressure vessels not only have the advantage of low weight and high strength but can also offer new opportunities to tailor stiffness distributions to achieve a desired structural behaviour by changing the fibre orientation spatially throughout the surface of the pressure vessel. This technique is often known as variable angle tow (VAT) and has been used by several researchers to achieve different design objectives [3–7]. Recently, Daghighi et al. [8] used VAT technology to suppress bending in super ellipsoids of revolution composite pressure vessels, noting that such shapes can approach cubic forms offering advantages in terms of packing efficiency, yet suffer surface bending in conventional metallic and composite designs as the vessel deforms to become spherical. In the bend-free design the load is uniformly distributed through the wall thickness. In other words, the in-plane stress gradient in the thickness direction is suppressed which results in mass reduction that can be beneficial for different applications.

Failure of pressurised vessels is deep rooted in history. Several vessel explosions causing damage ranged from minor to catastrophic happened in the early $1900s$ due to the lack of knowledge in standardisation in design, poor manufacturing techniques and material quality [1]. It is important to predict an accurate failure load for pressure vessels in order to have a safe design. Several researchers studied the failure of pressure vessels. Kam et al. [9] studied the first-ply failure strengths and burst strengths of composite pressure vessels with different lay-up configurations. In their study, depending on the lay-up, the Tsai-Wu failure criterion overpredicted first-ply failure pressure with an error between 12% to 25%. They also showed that the experimental first-ply failure pressure, depending on lay-up configuration, is 12% to 66% lower than the experimental ultimate burst pressure. However, they stated that the first-ply failure pressure can be appropriately used for design purposes. Chang [10] studied the first-ply failure strength of composite pressure vessels using both analytical and experimental approaches. He used maximum strain, Hoffman, Hill and Tsai-Wu failure criteria in order to find the first-ply failure strength of composite pressure vessels. In his study, depending on lay-up configuration, the Tsai-Wu failure criterion underpredicted the first-ply failure pressure with a 42% to 56% error. Onder et al. [11] assessed the effects of temperature and winding angle on burst pressure of filament wound composite pressure vessels. They considered composite pressure vessels with different stacking sequences given by $[\theta_1, -\theta_1]_s$ and suggested the optimum winding angle of 55° for their case study. They also showed that the burst pressure of composite pressure vessels depends on temperature as thermal stresses can affect the strength of the composite. Gohari et al. [12] investigated the effect of aspect ratio, thickness and stacking sequence on the first ply failure of an unsymmetrical laminated ellipsoidal composite shell under internal pressure. They used the first-ply Tsai-Wu failure criterion

to find the critical internal pressure. Based on their finding, the Tsai-Wu failure criterion overpredicted the first-ply failure pressure with approximately a 9% error. Their results suggest that results are more sensitive to thickness than stacking sequence and smaller thickness accounts for higher critical stress. Rafiee et al. [13] predicted the burst pressure in composite pressure vessels using first-ply-failure and compared the results against different failure criteria. In their study, they accounted for manufacturing uncertainties by considering the fibre volume fraction, winding angle and mechanical and strength properties as random parameters. Finally, they validated their results using experimental data. Their findings suggest that the Tsai-Wu failure criterion, depending on the lay-up configuration, underpredicted the first-ply failure pressure of the composite vessels without liner with an error between 13% to 28%.

From the literature, we note that two studies show that failure is overestimated by the 2D Tsai-Wu failure criterion and two studies also show it underestimated initial failure, both by amounts more than 10%. As such, one of the current aims is to examine 3D effects (material properties and stresses) on initial failure, noting that through-thickness stresses can be significant in laminated pressure vessels.

Daghighi et al. [14] conducted a failure analysis that revealed an exceptional performance for their proposed bend-free VAT design pressure vessel in comparison with isotropic and conventional composite pressure vessels comprising straight fibre trajectories. They conducted a failure study based on the Tsai-Wu criterion. An improvement of 204% for maximum pressure to weight was found for a bend-free VAT design pressure vessel in comparison with the best conventional composite pressure vessel. This exceptional failure performance along with the benefits in terms of mass reduction arising from bend-free design makes it a potential candidate for designing the next generation of pressure vessels. However, to evaluate the failure performance of bend-free VAT designed pressure vessels in greater detail and more accurately, a failure criterion that also accounts for through-thickness stresses should be considered.

Regarding doubly-curved surfaces, then constant-width unidirectional tows cannot cover the whole surface area without generating gaps or overlaps, as can be understood by considering the non-zero Gaussian curvature of the surface. Therefore, regardless of being tow-steered or unidirectional, thickness variation is inevitable in doubly curved shells made by automated tow placement. However, thickness variation as a result of overlaps can be prevented by using the tow-dropping method [5] or potentially reduced by using the appropriate lay down speed during the manufacturing process [15]. Moreover, new developments in manufacturing technologies such as spreading tapes provides scope to potentially alleviate the thickness variation caused by gaps and overlaps [16–18]. Therefore, the prospect of manufacturing bend-free VAT pressure vessels using spread tape technology is not only viable but a distinct possibility that forms part of near-future plans for this study. Before this, and to assess potential performance, it is important to investigate numerically the behaviour of the structure in more detail.

In this study, an ellipsoidal pressure vessel is designed to be bend-free using the method described by Daghighi et al. [8, 14]. The first-ply failure is considered to find the maximum pressure before failure using Tsai-Wu and three-dimensional invariant-based criteria for bend-free pressure vessels and their counterpart pressure vessels made of conventional unidirectionally-reinforced composites [19]. The maximum pressures found by these two failure criteria are compared and a parametric study is performed in order to gain physical insight and understand how 3D material properties affects performance.

The paper continues by presenting the design of bend-free pressure vessels. Section 3 discusses the failure criteria used in this study and some insights into the numerical modelling methods are provided in Section 4. Results obtained by the two failure criteria are presented in Section 5. A parametric study involving variations in material properties using a design of experiments approach are described in Section 6 and Subsections 6.1 to 6.3 present results of the parametric studies and finally in Section 8 a summary and conclusions are presented.

2. Bend-free design

A super ellipsoid of revolution is a particular geometry that can be expressed by [8]

$$\left[\left(\frac{x}{a}\right)^2+\left(\frac{y}{a}\right)^2\right]^{\frac{N}{2}}+\left(\frac{z}{b}\right)^N=1, \tag{1}$$

where a and b are two semi-axes as shown in Fig. 1 and N is the shape parameter representing the degree of sharpness at the corners. As N approaches infinity, the cross section in the $X-Z$ and $Y-Z$ planes becomes increasingly rectilinear. In this study, a special case of super ellipsoid of revolution with shape parameter $N=2$ (ellipsoid of revolution) and semi-major axis $a=0.5$ m is considered. The aspect ratio is considered to be the minimum allowable for the chosen material system, IM7/8552 carbon-epoxy, in order to remain a feasible bend-free design region ($K=b/a=0.72$) [14].

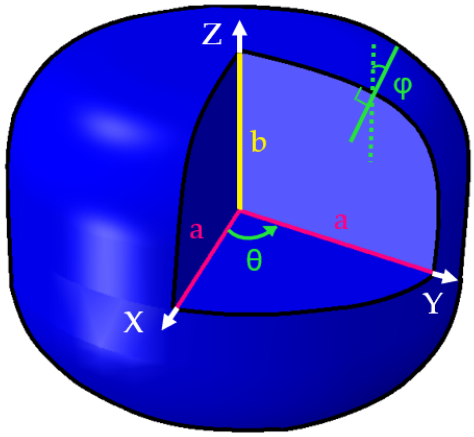

Fig. 1 Geometry of super ellipsoid of revolution.

In this study, IM7/8552 carbon epoxy material is used with material properties given in Table 1. Fibre volume is approximately 60% and the ply thickness is $h=0.15$ mm.

Table 1 Material properties for IM7/8552 carbon-epoxy prepreg.

Property	E_{11} GPa	E_{22} GPa	E_{33} GPa	G_{12} GPa	G_{13} GPa	G_{23} GPa	ν_{12} -	ν_{13} -	ν_{23} -
Value	161	11.38	11.38	5.2	5.2	3.9	0.32	0.32	0.45

The governing equation dictating the bend-free state of super ellipsoids of revolution under uniform internal pressure is expressed by [8]

$$-\Delta^2+2\Delta\left(\frac{U_1-U_4+U_2V_1^A+2U_3V_2^A}{U_1+U_2V_1^A+U_3V_2^A}\right)+\left(\frac{2U_4-U_1-3U_3V_2^A+U_2V_1^A}{U_1+U_2V_1^A+U_3V_2^A}\right)=0, \tag{2}$$

where U_1, U_2, U_3 and U_4 are material stiffness invariants, V_1^A and V_2^A are lamination parameters and Δ is

$$\begin{gathered}\Delta=\frac{r_\theta}{r_\varphi}=(N-1)\cdot K^{\frac{-N}{N-1}}\cdot\cos\varphi^{\frac{N-2}{N-1}}\cdot\left[\sin\varphi^{\frac{N}{N-1}}+(K\cos\varphi)^{\frac{N}{N-1}}\right],\\ K=\frac{b}{a}.\end{gathered} \tag{3}$$

Eq. 2 is used to tailor the stiffness through the structure. For a specific material system, then at each position in the structure identified by a specific value of φ, then solving Eq. 2 identifies a specific fibre orientation [8] that provides bend-free conditions. It is worth noting that, the structure is axisymmetric and therefore the value found for a specific φ is valid for all θ from 0° to 360°. Moreover, the fibre orientation remains constant for the locus equidistant from the equator. Considering a 4-ply balanced symmetric laminate, i.e. $[\theta_1, -\theta_1]_s$, then the desired fibre angle distribution (θ_1), is shown in Fig. 2. It is 45° at the poles and smoothly changes to 0° at the equator where there is the largest difference between the two geometrical radii of curvature.

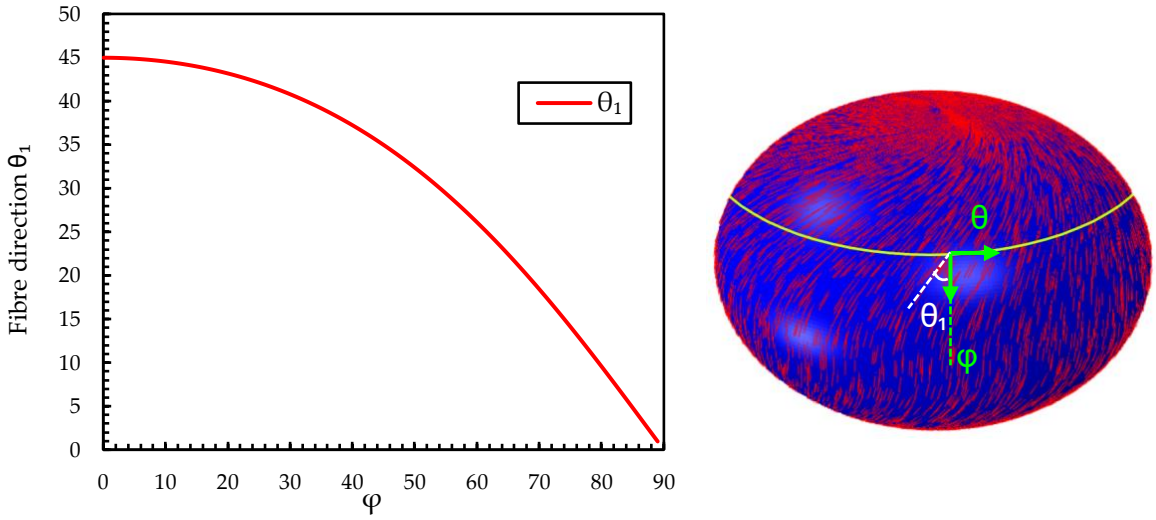

Fig. 2 Fibre angle distribution tailored for bend-free state.

3. Failure criteria

The maximum uniform internal pressure is to be found for the bend-free structure using both Tsai-Wu and three-dimensional invariant-based first-ply failure criteria. To gain more insight, considering a baseline geometry, the failure study identifies the maximum internal pressure for four structures with different constant fibre orientations ($\theta_1 = 0°$, 30°, 60° and 90°) with stacking sequence $[\theta_1, -\theta_1]_s$. Results were then compared with the maximum internal pressure found for the bend-free designed structure. First-ply failure, based on Tsai-Wu criterion occurs when

$$H_1\sigma_1 + H_2\sigma_2 + H_6\tau_{12} + H_{11}{\sigma_1}^2 + H_{22}{\sigma_2}^2 + H_{66}{\tau_{12}}^2 + 2H_{12}\sigma_1\sigma_2 < 1, \tag{4}$$

is not satisfied in a layer of the laminate. In Eq. 4, the coefficients of the Tsai-Wu failure criterion depend on material properties as

$$H_1 = \frac{1}{X_T} - \frac{1}{X_C}, \tag{5}$$

$$H_{11} = \frac{1}{X_T X_C}, \tag{6}$$

$$H_2 = \frac{1}{Y_T} - \frac{1}{Y_C}, \tag{7}$$

$$H_{22} = \frac{1}{Y_T Y_C}, \tag{8}$$

$$H_6 = 0, \tag{9}$$

$$H_{66} = \frac{1}{S_l^2}, \tag{10}$$

$$H_{12} = -\frac{1}{2X_T^2}, \tag{11}$$

where X_T, X_C, Y_T, Y_C and S_L are defined in Table 2. This criterion is evaluated for each ply using their stress states found numerically by Abaqus as described in Section 4.

Table 2 Material properties for IM7/8552 carbon-epoxy.

	Property	**Value**
X_T (MPa)	longitudinal tensile strength	2323.5
X_C (MPa)	longitudinal compressive strength	−1017.5
Y_T (MPa)	transverse tensile strength	62.3
Y_{BT} (MPa)	transverse tensile biaxial strength	38.7
Y_C (MPa)	transverse compressive strength	−253.7
Y_{BC} (MPa)	transverse compressive biaxial strength	−600.0
S_L (MPa)	in-plane shear strength	89.6
β (10^{-8}MPa^{-3})	parameter defining the nonlinearity of the shear stress-shear strain relation	2.12

In order to evaluate the failure performance in more detail, a three-dimensional invariant-based failure criterion that also accounts for through-thickness stresses is considered [19]. This failure criterion builds upon the invariance properties of a tensor which represents the material's intrinsic characteristic direction, as described by Vogler et al. [20] and therefore distinguishes between matrix-dominated and fibre-dominated failure mechanisms. In this method, transverse failure is directly formulated from invariant theory. The longitudinal tensile fracture is based on the non-interacting maximum allowable strain criterion as also used in [21–23] while longitudinal compressive failure is based on a three-dimensional kinking model that considers the nonlinear shear response which is known to occur in fibre-reinforced polymers [19, 24]. A flowchart summarising the three-dimensional invariant-based failure criterion is shown in Figs. 3 and 4.

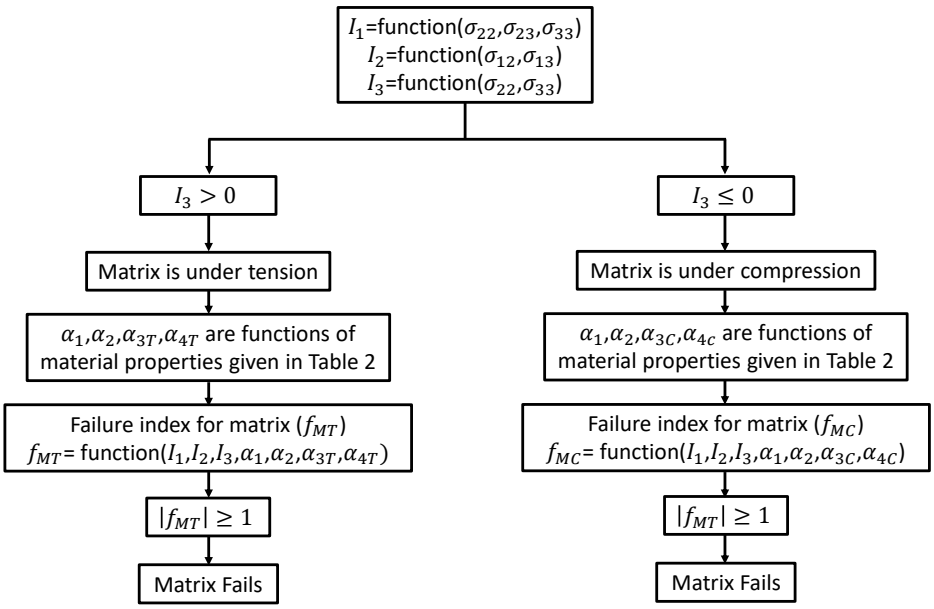

Fig. 3 Flowchart describing three-dimensional invariant-based failure criterion for matrix failure.

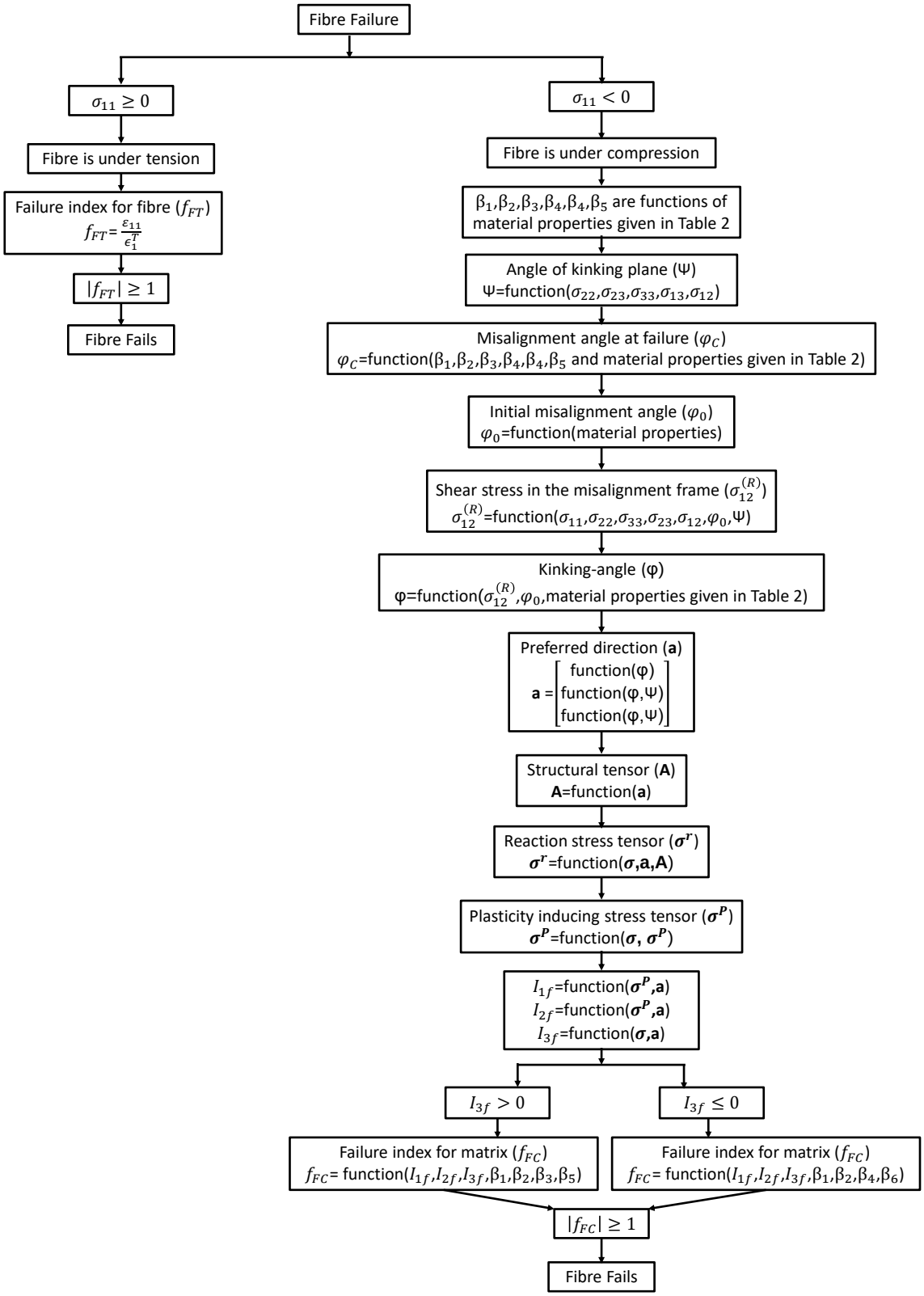

Fig. 4 Flowchart summarising three-dimensional invariant-based failure criterion for fibre failure.

4. Numerical modelling

Failure criteria were assessed by evaluating the stress state in each composite layer using ABAQUS [25] finite element analysis (FEA). The Tsai-Wu criterion is based on in-plane stresses while the three-dimensional invariant-based failure criterion is based on both in-plane and out-of-plane stresses. Super ellipsoids of revolution are axisymmetric structures and therefore stress states found for a strip in the φ direction are the same as those in the longitudinal direction.

The sub-modelling technique in ABAQUS was used to obtain the out-of-plane stresses in a computationally efficient way, as shown in Fig. 5. In this technique, only a small part of a model i.e. (sub-model) is studied with a refined mesh based on the interpolation of the solution obtained from the global model that was obtained with a relatively coarse mesh. The global model is discretised with triangular shell elements $S3$ (at its top and bottom) and quadrilateral shell elements $S4$ elsewhere. The sub-model was discretised with 8-node quadratic tetrahedral elements $C3D8I$, whilst at its top and bottom it was discretised with 6-node linear triangular prism elements $C3D6$. Distortional locking was minimised by optimising the in-plane aspect ratio of finite elements to be as close as possible to 1 [14]. Then, a mesh convergence study for choosing the number of solid elements through the thickness was performed to ensure that FEA results were not mesh size dependent and, as such, one solid element per layer with nine integration points was used in this study. Fig. 6 provides a flowchart describing the FEA approach taken.

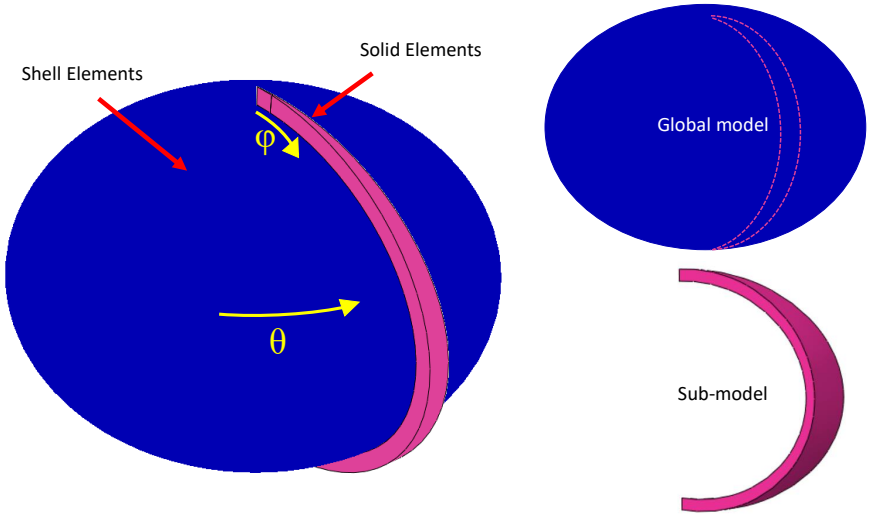

Fig. 5 Schematic of sub-modelling technique.

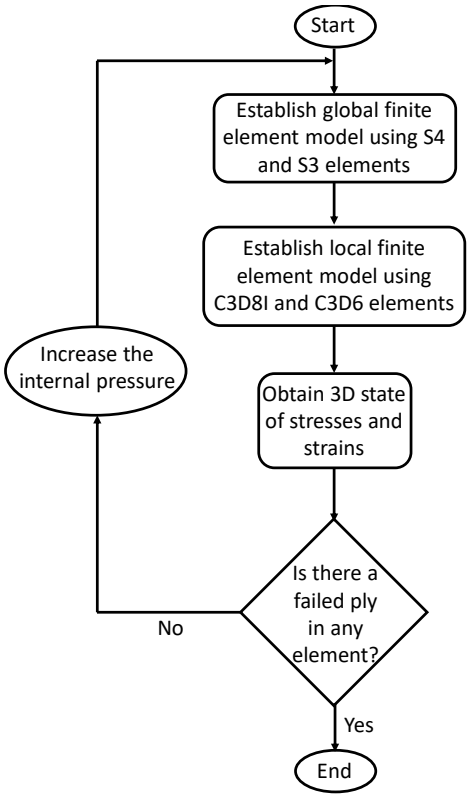

Fig. 6 Flow chart of finite element analysis.

5. Failure results

The maximum allowable internal pressure to weight ratios for the bend-free VAT designed structure and its counterpart structure with different constant fibre orientations are shown in Fig. 7 where unidirectionally reinforced composites with $[\theta_1, -\theta_1]_s$ are shown by θ_1. Based on these results, the VAT structure designed to be bend-free has better performance in failure in comparison with unidirectionally reinforced composite structures using both failure criteria. One plausible explanation for this behaviour is that the stresses and strains are uniformly distributed through the thickness which makes it possible to use the full load carrying potential of the structure.

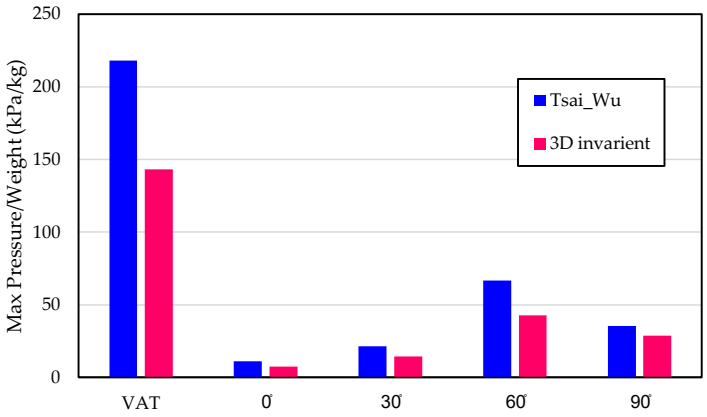

Fig. 7 The maximum allowable internal pressure to weight.

As shown in Fig. 7, the maximum allowable internal pressure found by the three-dimensional invariant-based failure criterion (P_{3D}) is lower than that found by the Tsai-Wu criterion (P_{TW}). The failure load reduction percentage ($R_{\%}$) can be assessed by

$$R_{\%} = \frac{P_{TW} - P_{3D}}{P_{TW}} \times 100. \tag{12}$$

Fig. 8 shows $R_{\%}$ for all studied structures. As shown in Fig. 8, $R_{\%}$ is on average around 30%. This reduction is due to the fact that the three-dimensional invariant-based failure uses both in-plane and out-of-plane stresses and strains of each ply in the multidirectional laminates and therefore is more comprehensive in its prediction in comparison to the Tsai-Wu criterion, which only considers in-plane stresses.

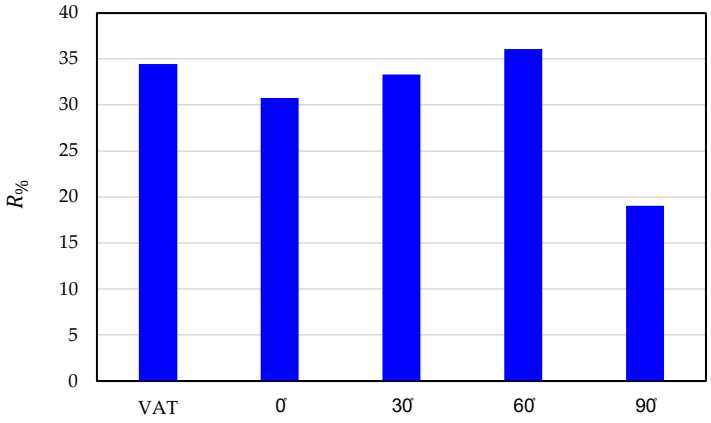

Fig. 8 $R_{\%}$ for different structures.

Using the three-dimensional invariant-based failure criterion makes it possible to distinguish between matrix-dominated failure and fibre-dominated failure mechanisms. It can also identify whether matrix and fibre are under tension or compression as shown in Figs. 9 to 11 for each structure. As shown in Fig. 9, both fibres and matrix in the fourth layer (outer layer) of the 0° structure are under compression at the poles while they are under tension elsewhere. For the 30° structure, as shown in Fig. 9, fibres are only under compression in the fourth layer around the poles. However, the matrix is under compression in all layers near the equator and in the fourth layer at the poles. Fig. 10 shows that both fibres and matrix are only under

compression in the first and second layers near the poles for the 60° and 90° structures. As shown in Fig. 11, both fibre and matrix in the VAT bend-free structure are under tension at all locations. This expected result is in agreement with the fact that the bend-free structure is both moment-less and curvature-less and therefore under uniform internal pressure, expands uniformly resulting in the laminate being under tension.

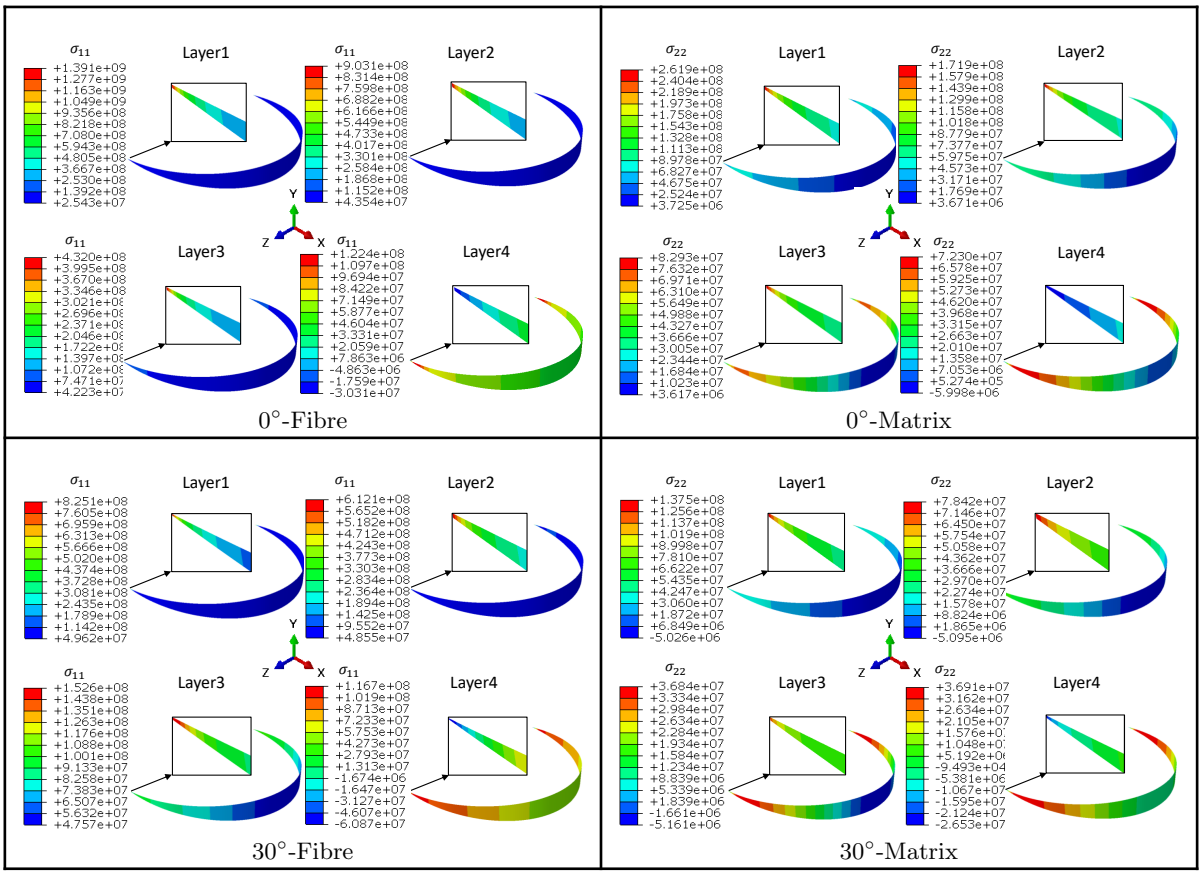

Fig. 9 Locations where fibre and matrix are under tension or compression in 0° and 30° structures. These values of stresses are obtained for uniform internal pressure of 100 kPa and are expressed in Pa.

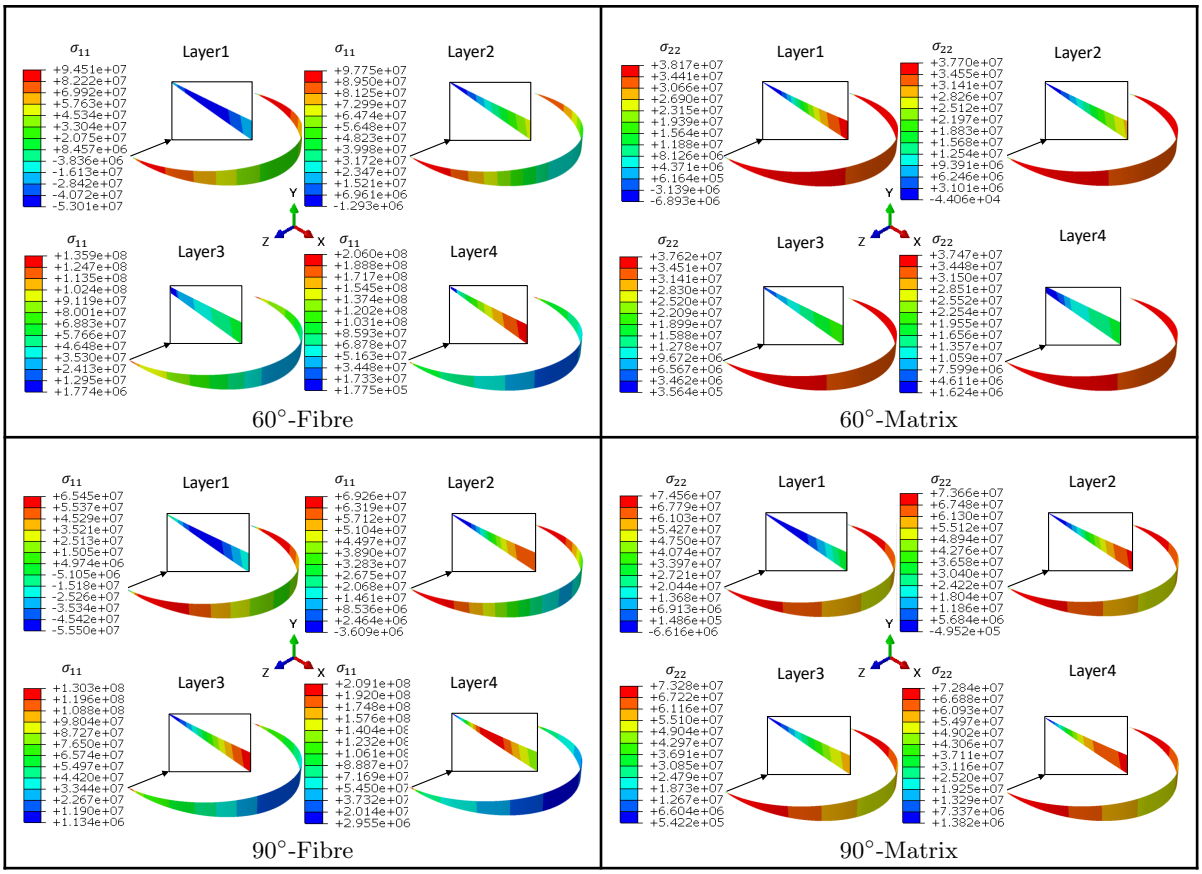

Fig. 10 Locations where fibre and matrix are under tension or compression in 60° and 90° structures. These values of stresses are obtained for uniform internal pressure of 100 kPa and are expressed in Pa.

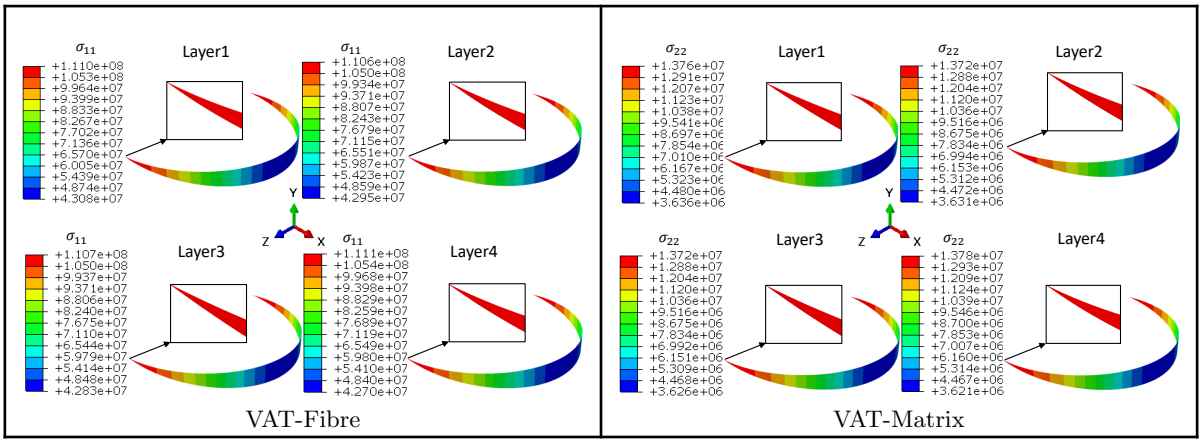

Fig. 11 Locations where fibre and matrix are under tension or compression in the VAT designed structure. These values of stresses are obtained for uniform internal pressure of 100 KPa and are expressed in Pa.

Table 3 shows the location in terms of φ and layer number where failure starts based on both criteria in each structure. Moreover, whether the structure is matrix or fibre failure dominant based on the three-dimensional invariant-based failure criterion, is indicated. As shown in Table 3, the location of failure is in

agreement for VAT, 0° and 30° structures based on both criteria. However, the failure locations based on the two criteria for 60° and 90° structures are near to each other but not exactly the same. Furthermore, failure in the VAT structure happens at layer 4 (outer layer), while for unidirectionally reinforced composites happens at Layer 1, i.e. the inner layer.

Table 3 Failure location.

Fibre orientation	**Tsai-Wu Failure**		**3-D Invariant-based Failure**		
	φ **(deg)**	**Layer**	φ **(deg)**	**Layer**	**Dominant failure mechanism**
0°	0.12	Layer 1	0.12	Layer 1	Matrix
30°	0.12	Layer 1	0.12	Layer 1	Matrix
60°	5.21	Layer 1	0.60	Layer 1	Fibre
90°	4.77	Layer 1	5.21	Layer 1	Matrix
VAT	0.13	Layer 4	0.13	Layer 4	Matrix

6. Parametric study and design of experiments

As shown in Section 5, the maximum allowable internal pressure found by the three-dimensional invariant-based failure criterion (P_{3D}) is on average about 30% lower than that predicted by the Tsai-Wu criterion (P_{TW}). In this section, the effects of material properties on the failure load reduction percentage ($R_{\%}$) is studied with a parametric study. Understanding the effects of material properties can provide more physical insights and be useful for designers especially regarding materials selection purposes. In this parametric study, a Taguchi design of experiments was used to minimise the number of virtual test runs and still be able to estimate the contribution of each factor [26, 27]. This is an efficient method that studies the entire space of factors with a small number of experiments. Taguchi design uses orthogonal arrays that are balanced and studies the effects of factors on the response. In this method factors are weighted equally and can be assessed independently.
This section is divided into three parts. The first part deals with the effects of five out-of-plane material properties on $R_{\%}$ that is discussed in Subsection 6.1. In the second part as described in Subsection 6.2, the effects of three material properties linked to strength on $R_{\%}$ are studied. These are the material properties that three-dimensional invariant-based failure criterion uses in addition to the material properties used in the Tsai-Wu criterion. Finally, Subsection 6.3 describes the parametric study that is performed between the most influential out-of-plane material property and the most influential material property linked to strength that are found in Subsections 6.1 and 6.2, respectively.

6.1. Parametric study on out-of-plane material properties linked to stiffness.

A parametric study is performed to evaluate the effect of five parameters including E_{33}, G_{13}, G_{23}, ν_{13} and ν_{23} on the failure load reduction percentage ($R_{\%}$). It should be noted that these five parameters are additional material properties that directly affect the out-of-plane stress state. To perform a parametric study, considering the factors with levels as described in Table 4, the Taguchi L_{16} orthogonal design table used is shown in Table 4.

Table 4 Factors and their levels for parametric study on out-of-plane material properties.

Factors	**Level** 1	**Level** 2	**Level** 3	**Level** 4
E_{33} (GPa)	8	12	16	20
G_{13} (GPa)	5	6	7	8
G_{23} (GPa)	3.5	4.4	5.3	6.2
ν_{13}	0.20	0.24	0.28	0.32
ν_{23}	0.25	0.32	0.39	0.46

Sixteen ellipsoidal pressure vessels were modelled and for each one, the out-of-plane material properties were changed as shown in Table 5 for each virtual test run. Failure analysis was performed based on the results obtained for each structure using solid elements in ABAQUS as described in Subsection 4. The failure load reduction percentage ($R_{\%}$), as described in Eq. 12, was determined for each structure and shown in Table 5.

Table 5 Taguchi L_{16} orthogonal design table for parametric study on out-of-plane material properties.

Virtual Test Run	**Factors**					**Results**
	E_{33} (GPa)	G_{13} (GPa)	G_{23} (GPa)	ν_{13}	ν_{23}	$R_{\%}$
1	8	5	3.5	0.20	0.25	21.83
2	8	6	4.4	0.24	0.32	24.35
3	8	7	5.3	0.28	0.39	26.59
4	8	8	6.2	0.32	0.46	28.67
5	12	5	4.4	0.28	0.46	34.98
6	12	6	3.5	0.32	0.39	33.94
7	12	7	6.2	0.20	0.32	29.17
8	12	8	5.3	0.24	0.25	27.89
9	16	5	5.3	0.32	0.32	37.59
10	16	6	6.2	0.28	0.25	33.98
11	16	7	3.5	0.24	0.46	40.18
12	16	8	4.4	0.20	0.39	37.02
13	20	5	6.2	0.24	0.39	42.80
14	20	6	5.3	0.20	0.46	44.30
15	20	7	4.4	0.32	0.25	40.00
16	20	8	3.5	0.28	0.32	41.44

Table 6 represents the mean response for each level of the factor. Delta represents the difference between the highest and lowest mean response values for each factor and rank is assigned based on the delta value. Rank of the factors those that have the largest effect on the response. As shown in Table 6, E_{33}, ν_{23}, ν_{13}, G_{23} and G_{13} are factors in the order that most affect the results, respectively. This trend is also shown in Fig. 12 that shows the highest variation of mean value of response for E_{33}, ν_{23}, ν_{13}, G_{23} and G_{13}, respectively. As shown in Fig. 12, the results are largely independent of G_{23} and G_{13}. Based on data shown in Fig. 12, loss of strength can be reduced by decreasing E_{33}, ν_{23} and ν_{13} and increasing G_{13} and G_{23}. It can be concluded that the difference of failure load between the two methods can be minimised by reducing levels of E_{33}, ν_{23} and ν_{13} and increasing levels of G_{23} and G_{13}.

Table 6 Mean response for parametric study on out-of-plane material properties.

Levels	E_{33}	G_{13}	G_{23}	ν_{13}	ν_{23}
1	25.36	34.30	34.35	33.08	30.93
2	31.50	34.14	34.09	33.80	33.14
3	37.19	33.99	34.09	34.25	35.09
4	42.14	33.76	33.66	35.05	37.03
Delta	16.78	0.54	0.69	1.97	6.11
Rank	1	5	4	3	2

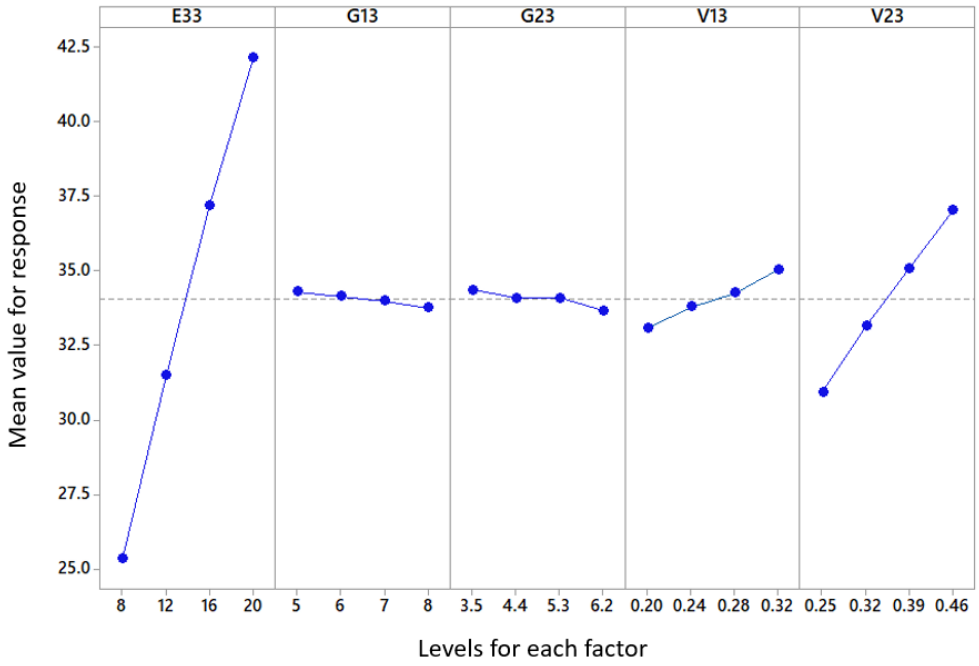

Fig. 12 Mean value of the response for each factor for parametric study on out-of-plane material properties.

6.2. Parametric study on material properties linked to strength.

A parametric study was performed in order to understand how material properties linked to strength including Y_{BT}, Y_{BC} and β affect $R_{\%}$. These are material properties linked to strength that are used additionally in the three-dimensional invariant-based failure criterion in comparison with the Tsai-Wu criterion. To perform a parametric study, three levels for each factor is considered as shown in Table 7. Full factorial design of experiment suggests 3^3 (27) virtual tests to study the effects of parameters. However, similar to the study undertaken in Subsection 6.1, a Taguchi design of experiments was used to reduce the number of required virtual tests.

Table 7 Factors and their levels for parametric study on material properties linked to strength.

Factors	**Level** 1	**Level** 2	**Level** 3
Y_{BT} (MPa)	16	33	50
Y_{BC} (MPa)	180	520	860
β (10^{-8}MPa^{-3})	0	2.30	4.6

Considering the factors with levels as described in Table 7, a Taguchi L_9 orthogonal design table is used as shown in Table 8. The three-dimensional invariant-based failure criterion was used to find the failure load of an ellipsoidal pressure vessel considering different material strength properties as described, for each virtual test, in Table 8. Numerical results, determined by solid elements in ABAQUS, as described in Subsection 4, inform the failure study. The parametric study is performed on the VAT bend-free designed structure, which is under tension everywhere and the unidirectionally reinforced composite with 60° fibre orientation, which is under tension or compression depending on the location in the structure, as discussed in Subsection 5. This effect is due to the fact that the three-dimensional invariant-based failure criterion is formulated such that depending on whether the fibre and matrix are under tension or compression, the criterion uses

only Y_{BT} or Y_{BC}. The failure load reduction percentage ($R_{\%}$), as expressed in Eq. 12, was found for each structure and shown in Table 8.

Table 8 Taguchi L_9 orthogonal design table for parametric study on material properties linked to strength.

Virtual Test Run	**Factors**			**Results**	
	Y_{BT} (MPa)	Y_{BC} (MPa)	β (10^{-8}MPa^{-3})	$R_{\%}$ VAT	$R_{\%}$ 60°
1	16	180	0	72.92	66.46
2	16	520	2.3	72.92	66.46
3	16	860	4.6	72.92	66.46
4	33	180	2.3	43.52	41.77
5	33	520	4.6	43.52	36.08
6	33	860	0	43.52	36.08
7	50	180	4.6	19.52	41.77
8	50	520	0	19.52	36.08
9	50	860	2.3	19.52	36.08

Tables 9 and 10 present the mean response for each level of the factor for the VAT bend-free and 60° structures, respectively. As shown in Table 9, based on the delta value, Y_{BT} influences the response most and the results are independent of Y_{BC} and β for the bend-free VAT designed structure, as explained by both fibres and matrix in the bend-free VAT designed structure being under tension and therefore based on the formulation of the three-dimensional invariant-based failure criterion, the only parameter used to study the failure among the considered factors in this parametric study is Y_{BT}. This effect is also shown in Fig. 13 that shows the largest variation of mean value of response for Y_{BT} and the results are independent of Y_{BC} and β. Based on data shown in Fig. 13, the difference in failure loads between the two methods for the VAT bend-free designed structure can be minimised by increasing levels of Y_{BT}.
However, considering the results shown in Table 10, Y_{BT}, Y_{BC} and β are factors in the most influential order that affect the results for the 60° structure, respectively. This effect is due to the fact that depending on the location, the structure is under tension or compression and therefore the criterion uses both Y_{BT} and Y_{BC} and, as a result, the response also depends on Y_{BC}. This influence is also shown in Fig. 14 where the largest variation of the mean value of response occurs for Y_{BT}. Based on data shown in Fig. 14, the difference in failure load between the two methods for the 60° structure can be minimised by increasing levels of Y_{BT} and Y_{BC}. However, increasing Y_{BC} beyond a certain level does not bear influence.

Table 9 Mean response for VAT in parametric study on material properties linked to strength.

Level	Y_{BT}	Y_{BC}	β
1	72.92	45.20	45.20
2	43.52	45.20	45.20
3	19.15	45.20	45.20
Delta	53.77	0.00	0.00
Rank	1	2.5	2.5

Table 10 Mean response for 60° in parametric study on material properties linked to strength.

Level	Y_{BT}	Y_{BC}	β
1	66.46	50.00	46.20
2	37.97	46.20	48.10
3	37.97	46.20	48.10
Delta	28.48	3.80	1.90
Rank	1	2	3

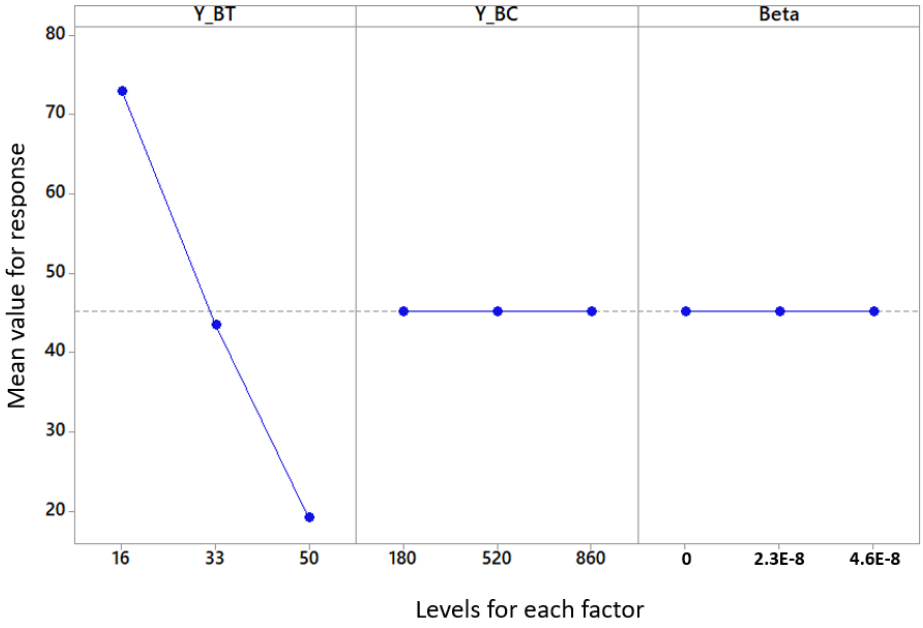

Fig. 13 Mean value of response for each factor in parametric study of VAT on material properties linked to strength.

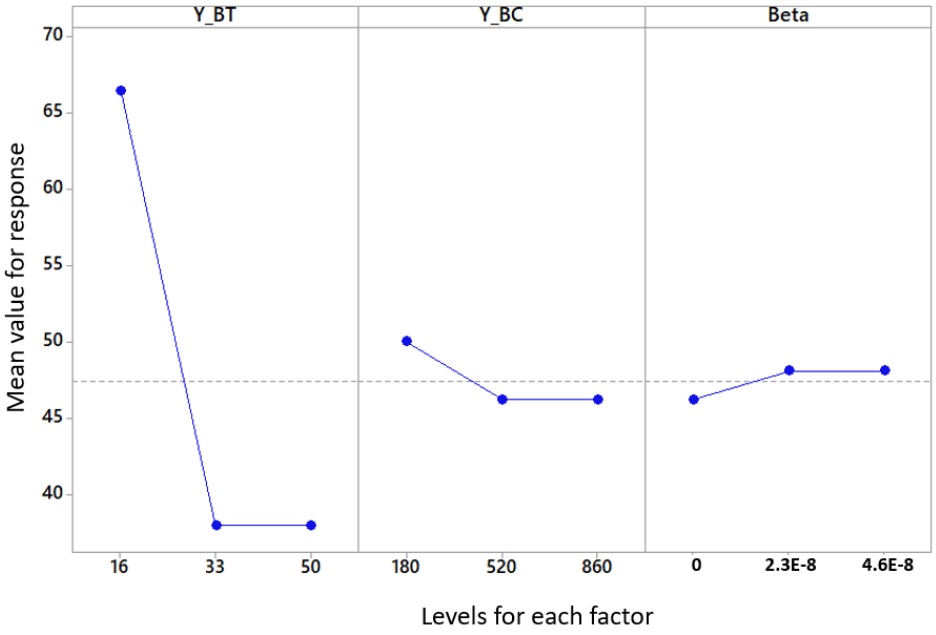

Fig. 14 Mean value of response for each factor in parametric study of 60° on material properties linked to strength.

6.3. Parametric study on most influential out-of-plane stiffness and strength material properties.

The parametric study described in Subsection 6.1, reveals that E_{33} is the out-of-plane stiffness material property that most affects $R_{\%}$. Moreover, based on the results shown in Subsection 6.2, among the additional material properties linked to strength, Y_{BT} has the largest effect on $R_{\%}$. Here, a parametric study is performed to identify between E_{33} and Y_{BT}, which influences $R_{\%}$ most. To perform a parametric study, four levels for each factor is considered as shown in Table 11.

Table 11 Factors and their levels for parametric studies on E_{33} and Y_{BT}.

Factors	**Level** 1	**Level** 2	**Level** 3	**Level** 4
E_{33} (GPa)	8	12	16	20
Y_{BT} (MPa)	17	28	39	50

Considering the factors with levels as described in Table 11, a Taguchi L_{16} orthogonal design table as shown in Table 12 is used to design the virtual tests and estimate the contribution of each factor. The three-dimensional invariant-based failure criterion was used to find the failure load of 16 VAT bend-free pressure vessels considering different E_{33} and Y_{BT} values, as described for each virtual test in Table 12. It is noted that the failure analysis was performed based on the results obtained for each structure using solid elements in ABAQUS. $R_{\%}$ was found for each structure and are shown in Table 12.

Table 12 Taguchi L_{16} orthogonal design table for parametric studies on E_{33} and Y_{BT}.

Virtual Test Run	**Factors**		**Results**
	E_{33} (GPa)	Y_{BT} (MPa)	$R_{\%}$
1	8	17	68.46
2	8	28	81.63
3	8	39	28.08
4	8	50	16.29
5	12	17	71.74
6	12	28	83.79
7	12	39	34.98
8	12	50	19.76
9	16	17	74.26
10	16	28	85.42
11	16	39	40.77
12	16	50	24.60
13	20	17	76.33
14	20	28	86.70
15	20	39	45.74
16	20	50	30.31

Table 13 presents the mean response for each factor level. As shown in Table 13, based on delta values, Y_{BT} and E_{33} influence results most (in decreasing order). This trend is also shown in Fig. 15 that shows the largest variation of the mean value of response for Y_{BT}. Based on data shown in Fig. 15, the minimum amount for $R_{\%}$ can be obtained at the fourth level of Y_{BT} and the first level of E_{33}. It can be concluded that the difference in failure loads between the two methods for the VAT bend-free designed structure can be minimised by increasing levels of Y_{BT} and decreasing levels of E_{33}. It is worth nothing that as shown in Fig. 15, increasing the level of Y_{BT} from the first to the second level increases $R_{\%}$ but then its trend changes and increasing the level of Y_{BT} results in reducing $R_{\%}$.

Table 13 Mean response for parametric studies on E_{33} and Y_{BT}.

Level	E_{33}	Y_{BT}
1	48.61	72.70
2	52.57	84.39
3	56.26	37.39
4	59.77	22.74
Delta	11.16	61.65
Rank	2	1

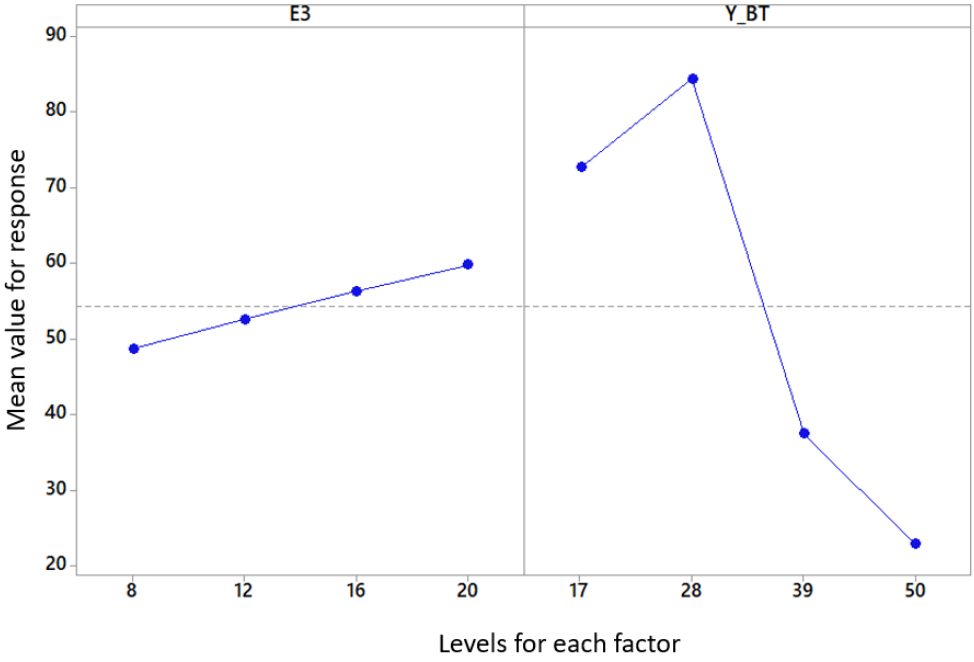

Fig. 15 Mean value of response for each factor in parametric study on E_{33} and Y_{BT}.

7. Effect of 3D stresses on bend-free design

The bend-free governing equation for super ellipsoids of revolution as described by Daghighi et al. [8], is based on 2D stresses and strains and only considers in-plane stresses to design bend-free pressure vessels. However, it is interesting to study the through-thickness stress, σ_{33}, in bend-free vessels and compare them against conventional composite vessels. Fig. 16 shows σ_{33} for bend-free and conventional unidirectionally-reinforced composite vessels in each layer. As shown in Fig. 16, the bend-free composite vessel has the lowest amount of through-thickness stress, σ_{33}. In other words, the stress is distributed more uniformly through the structure. Moreover, σ_{33} in the bend-free VAT vessel is almost constant for all layers through the structure. However, this is not valid for all locations in conventional composite vessels. Comparing the results for σ_{33}, shown in Fig. 16, with maximum allowable internal pressure, shown in Fig. 7, suggests that the vessel with more uniformly distributed σ_{33} through the structure, carries the highest internal pressure. Therefore, bend-free VAT vessel, 60°, 90°, 30° and 0° structures are in the order that carry the highest internal pressure.

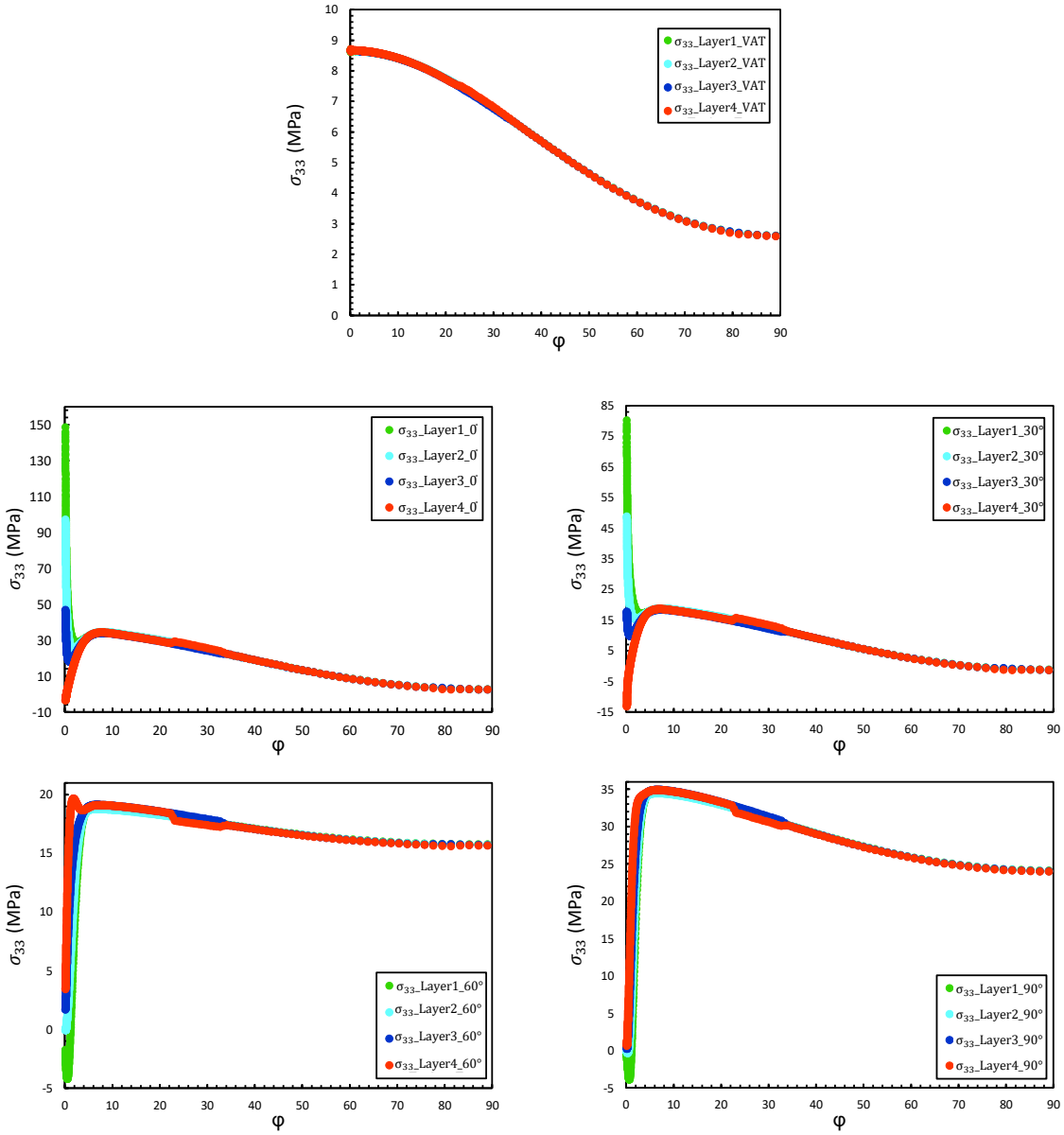

Fig. 16 Through-thickness stress, σ_{33}, plots in φ direction.

8. Summary and conclusion

A bend-free ellipsoidal pressure vessel has been designed by tailoring the stiffness using fibre steering methods. Failure performance of the bend-free design was subsequently evaluated using both Tsai-Wu and three-dimensional invariant-based criteria. The maximum pressure before failure of the bend-free design was compared with results for its counterpart pressure vessel made from different unidirectionally reinforced composites. Results confirm the finding of Daghighi et al. [14] that the bend-free design has the best failure performance in comparison with other unidirectionally reinforced composites using both Tsai-Wu and

three-dimensional invariant-based criteria. The maximum allowable internal pressure predicted by the three-dimensional invariant-based failure criterion (P_{3D}) for bend-free VAT vessel is 34% lower than the amount found by the Tsai-Wu criterion (P_{TW}). However, this failure load reduction for conventional unidirectionally-reinforced composite vessels is on average approximately 30%.
A parametric study on material stiffness properties shows that E_{33}, ν_{23}, ν_{13}, G_{23} and G_{13} in decreasing order are most influential in reducing failure loads in comparison to 2D failure criteria. Additionally, loss of strength can be reduced by decreasing E_{33}, ν_{23} and ν_{13} and by increasing G_{23} and G_{13}. A parametric study was also performed to study the effects of additional material properties linked to strength and based on these results, Y_{BT} was shown to have the largest effect and increasing Y_{BT} levels reduces loss of strength. Finally, a parametric study on the most influential out-of-plane material stiffness property (E_{33}) and the most influential material property linked to strength (Y_{BT}) was performed and shows that Y_{BT} has the largest effect on strength loss linked to 3D effects and that can be minimised by increasing Y_{BT} and decreasing E_{33} values. Finally, through-thickness stress, σ_{33}, in bend-free vessels was compared against conventional unidirectionally-reinforced composite vessels. Results show that σ_{33} is distributed more uniformly through the structure in the bend-free VAT vessel in comparison with conventional unidirectionally-reinforced composite vessels. Furthermore, the combination of findings suggests that vessels with uniformly distribution of σ_{33} can carry higher internal pressure. The findings in this study, provide useful insight into bend-free pressure vessels and highlight their potential performance in terms of maximum allowable failure pressure. Moreover, our parametric studies identify physical insight that can be useful for material selection purposes. In other words, where possible, designers can perform materials selection by giving priority to Y_{BT}, E_{33}, ν_{23}, ν_{13}, G_{23} and G_{13}, respectively. As such, materials with larger Y_{BT}, G_{23} and G_{13} and smaller E_{33}, ν_{23}, ν_{13} are of interest. Overall, results show the benefits of using bend-free designs for the next generation of pressure vessels. Further research should be undertaken to verify experimentally current numerical results which forms part of future plans for this study.

Acknowledgement

The authors would like to thank Science Foundation Ireland (SFI) for funding Spatially and Temporally VARIable COMPosite Structures (VARICOMP) Grant No. (15/RP/2773) under its Research Professor programme.

References

[1] B. E. Ball, W. J. Carter, CASTI Guidebook to ASME Section VIII Div. 1-Pressure Vessels, CASTI Pub., 2004.

[2] M. LeGault, The first commercial type v composite pressure vessel (March 2020).
URL https://www.compositesworld.com/articles/next-generation-pressure-vessels

[3] M. M. Abdalla, S. Setoodeh, Z. Gürdal, Design of variable stiffness composite panels for maximum fundamental frequency using lamination parameters, Composite Structures 81 (2) (2007) 283 – 291.

[4] H. Akhavan, P. Ribeiro, Natural modes of vibration of variable stiffness composite laminates with curvilinear fibres, Composite Structures 93 (11) (2011) 3040 – 3047.

[5] C. Lopes, P. Camanho, Z. Gürdal, B. Tatting, Progressive failure analysis of tow-placed, variable-stiffness composite panels, International Journal of Solids and Structures 44 (25) (2007) 8493 – 8516.

[6] F. S. Liguori, G. Zucco, A. Madeo, D. Magisano, L. Leonetti, G. Garcea, P. M. Weaver, Postbuckling optimisation of a variable angle tow composite wingbox using a multi-modal koiter approach, Thin-Walled Structures 138 (2019) 183 – 198.

[7] M. Rouhi, H. Ghayoor, S. V. Hoa, M. Hojjati, Multi-objective design optimisation of variable stiffness composite cylinders, Composites Part B: Engineering 69 (2015) 249 – 255.

[8] S. Daghighi, G. Zucco, M. Rouhi, P. M. Weaver, Bend-free design of super ellipsoids of revolution composite pressure vessels, Composite Structures 245 (2020) 112283.

[9] T. Kam, Y. Liu, F. Lee, First-ply failure strength of laminated composite pressure vessels, Composite Structures 38 (1) (1997) 65 – 70, ninth International Conference on Composite Structures.

[10] R. Chang, Experimental and theoretical analyses of first-ply failure of laminated composite pressure vessels, Composite Structures 49 (2) (2000) 237 – 243.

[11] A. Onder, O. Sayman, T. Dogan, N. Tarakcioglu, Burst failure load of composite pressure vessels, Composite Structures 89 (1) (2009) 159 – 166.

[12] S. Gohari, S. Sharifi, Z. Vrcelj, M. Y. Yahya, First-ply failure prediction of an unsymmetrical laminated ellipsoidal woven gfrp composite shell with incorporated surface-bounded sensors and internally pressurised, Composites Part B: Engineering 77 (2015) 502 – 518.

[13] R. Rafiee, M. A. Torabi, Stochastic prediction of burst pressure in composite pressure vessels, Composite Structures 185 (2018) 573–583.

[14] S. Daghighi, M. Rouhi, G. Zucco, P. M. Weaver, Bend-free design of ellipsoids of revolution using variable stiffness composites, Composite Structures (2019) 111630.

[15] G. Clancy, D. Peeters, V. Oliveri, D. Jones, R. M. O'Higgins, P. M. Weaver, A study of the influence of processing parameters on steering of carbon fibre/peek tapes using laser-assisted tape placement, Composites Part B: Engineering 163 (2019) 243 – 251.

[16] G. Clancy, D. Peeters, R. M. O'Higgins, P. M. Weaver, In-line variable spreading of carbon fibre/thermoplastic pre-preg tapes for application in automatic tape placement, Materials & Design 194 (2020) 108967.

[17] G. J. Clancy, R. O'Higgins, P. M. Weaver, Spreading of carbon fiber/thermoplastic pre-preg tapes, in: AIAA Scitech 2020 Forum, 2020.

[18] G. Clancy, R. M. O'Higgins, P. M. Weaver, Carbon fibre/thermoplastic tape spreader, UK Patent application No:1904264.7 (Filed 27th March 2019).

[19] P. Camanho, A. Arteiro, A. Melro, G. Catalanotti, M. Vogler, Three-dimensional invariant-based failure criteria for fibre-reinforced composites, International Journal of Solids and Structures 55 (2015) 92 – 107.

[20] M. Vogler, R. Rolfes, P. Camanho, Modelling the inelastic deformation and fracture of polymer composites – part i: Plasticity model, Mechanics of Materials 59 (2013) 50 – 64.

[21] C. G. Davila, P. P. Camanho, C. A. Rose, Failure criteria for frp laminates, Journal of Composite Materials 39 (4) (2005) 323–345.

[22] G. Catalanotti, P. Camanho, A. Marques, Three-dimensional failure criteria for fibre-reinforced laminates, Composite Structures 95 (2013) 63 – 79.

[23] A. Puck, H. Schürmann, Chapter 5.6 - failure analysis of frp laminates by means of physically based phenomenological models, in: M. Hinton, A. Kaddour, P. Soden (Eds.), Failure Criteria in Fibre-Reinforced-Polymer Composites, Elsevier, Oxford, 2004, pp. 832 – 876.

[24] H. T. Hahn, S. W. Tsai, Nonlinear elastic behavior of unidirectional composite laminae, Journal of Composite Materials 7 (1) (1973) 102–118.

[25] ABAQUS/Standard User's Manual, Version 2017, Simulia, 2016.

[26] G. Taguchi, S. Chowdhury, Y. Wu, Taguchi's quality engineering handbook, New Jersey (2005).

[27] R. K. Roy, Design of experiments using the Taguchi approach: 16 steps to product and process improvement, John Wiley and Sons, 2001.